Radiant flux density, energy density and fuel consumption in mixed-oak forest surface fires

R. L. Kremens[A,D], *M. B. Dickinson*[B] *and A. S. Bova*[A,B,C]

[A]Rochester Institute of Technology, Center for Imaging Science, 54 Lomb Memorial Drive,
  Rochester, NY 14623 USA.
[B]US Forest Service Northern Research Station, 359 Main Road, Delaware, OH 43015, USA.
[C]Current address: Bova Consulting, 323 Northridge Road, Columbus, OH 43214, USA.
[D]Corresponding author. Email: kremens@cis.rit.edu

Abstract. Closing the wildland fire heat budget involves characterising the heat source and energy dissipation across the range of variability in fuels and fire behaviour. Meeting this challenge will lay the foundation for predicting direct ecological effects of fires and fire–atmosphere coupling. In this paper, we focus on the relationships between the fire radiation field, as measured from the zenith, fuel consumption and the behaviour of spreading flame fronts. Experiments were conducted in 8×8-m outdoor plots using preconditioned wildland fuels characteristic of mixed-oak forests of the eastern United States. Using dual-band radiometers with a field of view of $\sim 18.5\,\mathrm{m}^2$ at a height of 4.2 m, we found a near-linear increase in fire radiative energy density over a range of fuel consumption between 0.15 and 3.25 $\mathrm{kg\,m}^{-2}$. Using an integrated heat budget, we estimate that the fraction of total theoretical combustion energy density radiated from the plot averaged 0.17, the fraction of latent energy transported in the plume averaged 0.08, and the fraction accounted for by the combination of fire convective energy transport and soil heating averaged 0.72. Future work will require, at minimum, instantaneous and time-integrated estimates of energy transported by radiation, convection and soil heating across a range of fuels.

Introduction

The wildland fire grand measurement challenge can be described as integration of pre-, active- and post-fire measurements and physical process models into a robust and well-validated framework for characterising coupled fire–atmosphere dynamics, fire emissions and direct ecological effects at a range of scales from flame fronts to prescribed and wildfire events (Kremens *et al.* 2010). Significant progress has been made in developing measurement technologies for describing the convective (e.g. Banta *et al.* 1992; Coen *et al.* 2004; Clements 2007) and radiation fields at scales from the laboratory (Freeborn *et al.* 2008), to the event (Radke *et al.* 2000; Riggan *et al.* 2004) and to the region (Roberts *et al.* 2005). However, a comprehensive set of measurements linking energy release from fuel consumption in spreading fires with the various modes of heat dissipation has not been conducted. Convective (sensible) heat flux accounts for the largest fraction of heat dissipation, followed by radiant flux and then by soil and latent heat fluxes (e.g. Wooster *et al.* 2005; Freeborn *et al.* 2008). Unlike measurement of other modes of heat transport, quantifying the radiation field is possible at high spatial and temporal resolution and over large spatial extents.

The spatial and temporal pattern of radiant heat release from the combustion of wildland fuels (i.e. the radiation field) has been described at a range of scales. Wooster *et al.* (2005) and

Freeborn *et al.* (2008) describe the relationship between total and rates of combustion and fire radiative power (FRP, kW) and energy (FRE, kJ) from the flaming and smouldering phases of small-scale ($\sim 1\,\mathrm{m}$, subpixel) fires in the field and laboratory. Riggan *et al.* (2004) quantify the fire radiative flux density (FRFD) field at ~ 1-km scale from a fixed-wing aircraft whereas Radke *et al.* (2000) demonstrate the feasibility of quantifying fire radiative energy density (FRED) at a similar scale from continuous fire observation from a fixed-wing aircraft. Roberts and Wooster (2008) describe regional-scale FRE estimated with a geostationary satellite. Work linking the radiation field to fuel combustion dynamics on the ground (Wooster *et al.* 2005; Freeborn *et al.* 2008) has been motivated by the potential for using infrared radiation sensors on satellites (particularly geostationary satellites) to quantify biomass combustion over regional (e.g. Kaufman *et al.* 1996; Roberts *et al.* 2005) and landscape scales (e.g. Riggan *et al.* 2004; Kremens *et al.* 2010).

Experiments have quantified the coupling between fire heat release and atmospheric dynamics at a range of scales. Clements *et al.* (2008) described strong turbulence generated by prescribed fires in grass fuels and documented strong downdrafts after the flaming front had passed their observing apparatus. Coen *et al.* (2004) and Clark *et al.* (1999) used high-frequency infrared imagery to describe convective fluxes in and around crown fires. At an event scale, Banta *et al.* (1992) used Doppler

LiDAR (Light Detection and Ranging) and RADAR (Radio Detection and Ranging) to characterise the convective columns above a wildfire and prescribed fire, providing information that has the potential to be linked to descriptions of heat dissipation near source as quantified by remote infrared imaging. Again at event scales, Radke *et al.* (2000) used infrared imaging from an airborne platform to describe convective heat flux dynamics in high-intensity fires.

Missing are studies that take an integrated view of heat generation and dissipation in spreading fires. Except for Freeborn *et al.* (2008) at a $\sim$1-m scale in the laboratory, there have not been any simultaneous measurements of heat generation and dissipation by radiation and convection. Wooster *et al.* (2005) estimated soil heat flux along with radiative heat dissipation in non-spreading outdoor fires whereas Clements *et al.* (2006) calculated latent heat flux along with convective heat dissipation in spreading fires. Our study advances the integrative goal by examining fuel consumption (heat generation) and radiative heat transport for spreading, plot-scale fires and uses an integrated heat budget to guide thinking about future experiments.

Integrated heat budget

Consider a control volume that encloses the fuel, flames, heated air and combustion gas products (convective plume) and soil heated by the fire. All of the energy generation from combustion is contained in this volume (Fig. 1). A 'coarse' heat budget for the control volume roughly balances heat sources, sinks and dissipation integrated over the time period from ignition to the cool-down of the control volume to ambient temperatures:

$$Wh_C(1 - \varphi) = WQ_P + \text{FLED} + \text{FRED} + \text{FCED} + E_S \quad (1)$$

where W is the areal fuel consumption on a moisture and ash-free basis (kg m^{-2}); h_C is the high heat of combustion (i.e. includes heat of condensation of water generated by the combustion process, MJ kg^{-1}); φ is the fractional reduction in h_C because of incomplete combustion, $h_C(1 - \varphi)$ is the effective heat of combustion (Dietenberger 2002; Babrauskas 2006); Q_P is the fuel pre-heating and pyrolysis enthalpy (MJ kg^{-1}, defined so as not to include the fuel moisture vaporisation enthalpy, see below); FLED is the fire latent energy density (MJ m^{-2}), the condensation energy in water vapour generated from both fuel moisture and the combustion process; FRED is the fire radiative energy density (MJ m^{-2}), i.e. the FRFD time-integrated over the period from ignition to cool-down; FCED is fire convective energy density transported by the buoyancy-driven rise of heated combustion products and directly heated air; and E_S is the areal energy density transferred into the soil (MJ m^{-2}). Both sides of Eqn 1 have units of areal energy density, MJ m^{-2}. The left side of Eqn 1 is the energy available to do work near the fire front. All quantities involving fuel mass (e.g. consumption, heats of combustion) are on an ash- and moisture-free basis.

We estimate FRFD by measuring the radiation flux density that reaches a remote detector. The radiation that reaches the detector is modified by the presence of intervening objects or atmosphere that absorb, reflect or scatter radiation within the field of view of the detector. For example, some of the radiation from the fire may preheat the fuel and the soil surface around the
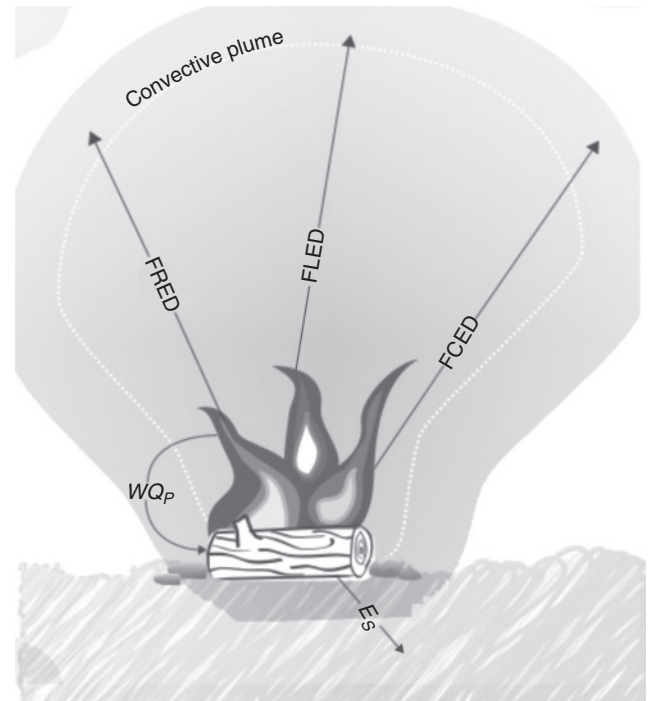

Fig. 1. Coarse energy partition during wildland fire combustion where the entire combustion zone is contained within the control volume. FRED, fire radiated energy density; FLED, fire latent energy density; FCED, fire convective energy density; E_S, energy transmitted to soil by conduction; WQ_P, fuel consumption–pyrolysis enthalpy product.

fire. If this heated soil and fuel is within the field of view of the detector, radiation emitted from the soil and fuel will be detected as a component of the FRFD. There are many other radiation transport paths but in all cases, the radiation that is finally measured at a remote detector will be less intense than would have been measured without these confounding elements. This experiment is designed to be equivalent to an overhead observation of the fire and without further experiments, we cannot determine the fraction of radiation lost to these dissipative processes.

Measurement strategy

A primary goal for this study was to provide the linkage between the radiation field and fuel consumption at the pixel scale needed to produce maps of FRFD and FRED from time-sequenced infrared imagery of wildland fires collected from a sensor on a fixed-wing aircraft. Our general measurement philosophy relative to quantifying the radiation field at event scales is outlined in Fig. 2, wherein a constrained fire heat budget is applied to predicting direct ecological effects. We begin (on the top of Fig. 2) with an instrument measuring some physical parameter (primarily, for this paper, radiant emission) that is calibrated against a secondary laboratory standard and whose strengths and limitations are well understood by extensive study in the laboratory. We then use these instruments on a finely controlled 'plot'-scale experiment where many relevant parameters (like local weather, fuel loading, fuel moisture and arrangement of fuels) can be measured and controlled. The calibrated instruments are used at this scale to measure the parameter of interest
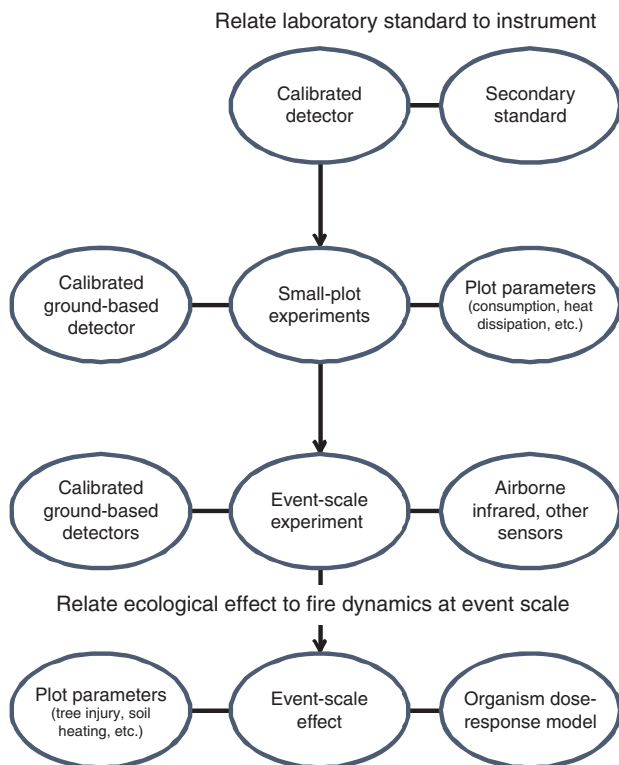
Relate laboratory standard to instrument

Fig. 2. A schematic outline of the experimental series of which this paper forms a part. The ultimate goal of the experimental series is the prediction of various ecological effects from fire heat-release maps derived from airborne or satellite imagery.
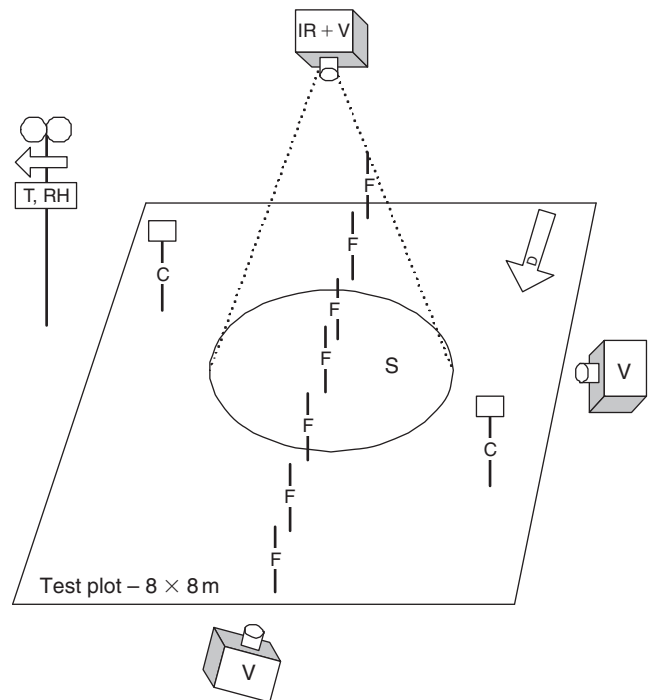

Fig. 3. Overhead schematic diagram of the plot layout indicating position of the primary diagnostics and field of view of the IR instrument. Key: S, sampled area; F, fiducial marker poles (only one dimension shown); C, carbon monoxide sensors; T, RH, weather station measuring wind speed, direction, air temperature and relative humidity; IR + V, overhead two-band IR detector plus video camera; V, orthogonal-axis video cameras; D, direction of prevailing wind and fire spread.

compared with the measured plot parameters. These plot-scale experiments are designed to have the same scale as the ground sampling distance (GSD) of our airborne fire observation system. In a future paper, we will discuss the expansion of the spatial scale of our measurement series from plots ($\sim$100 m^2) to events ($\sim$10^6 m^2) by using a combination of in-fire sensors similar to that used on the 'plot'-level fires combined with time-sequence airborne infrared imagery. Linking fire heat release with ecological effects is discussed in Dickinson and Ryan (2010) and associated papers.

Methods

Our experiments involved outdoor, spreading fires at a plot scale that link fuel consumption with the radiation field and provide definition and partial quantification of the integrated heat budget (Eqn 1). Measurements described fuel spread uniformly over 8 × 8-m plots, fuel consumption, fire spread behaviour, windward fire weather and the radiation field over $\sim$18.5 m^2 using overhead, single-pixel dual-band radiometers mounted on a tower.

The test fires were conducted at the Vinton Furnace State Experimental Forest in south-eastern Ohio, USA. Fuels were leaf litter from oak-dominated stands, downed woody material from the same stands and kiln-dried (untreated) conifer lumber redimensioned to 2.4 cm × 2.4 cm × 2 m. Bova and Dickinson (2008) provide further details on fuels and other aspects of these

plot fires. The kiln-dried lumber augmented downed woody material that was found to be insufficiently cured at the time of the experiments, resulting in consumption limited to small-diameter branches. The litter fuels were stored and cured in a large, heated warehouse. The fuels were arranged uniformly on the plot after being weighed so that the areal fuel loading (kg m^{-2}) was accurately known. Fuel moisture (as a fraction of dry weight) was determined on randomly selected subsamples.

Weather data (wind speed and direction, relative humidly and air temperature) were taken at 5-s intervals by a weather station located $\sim$3 m from the edge of the plot on the (generally) upwind side. Fuel moisture was estimated for all fuel classes based on samples collected just before ignition as described in Bova and Dickinson (2008). Diagnostics for these experiments were a three-view visible video camera system to monitor the position and height of visible flames, 2-m witness poles placed in a regular horizontal pattern and also marked at regular intervals along their length to measure the location and height of the flames, and a two-band infrared radiometer mounted 4.2 m above the centre of the plot. An array of thermocouples was arranged around the plot so that the time of arrival of the fire could be determined by a rapid rise in temperature of the thermocouple. All instruments were synchronised with the global positioning system (GPS) clock to assure simultaneous measurements. A diagram of the plot configuration is given in Fig. 3.

The primary diagnostic instrument for this experiment was a two-band infrared radiometer. The radiometer was mounted on a tower pointed towards the centre of the plot at a height of 4.2 m. The instrument has a view angle of 60°, and when mounted at this height, receives radiation from a circle of 4.8-m diameter on the ground (Fig. 3). The plot was purposely designed to be larger than the radiometer field of view so that edge effects would be avoided. A two-band radiometer has several advantages over a single-band instrument (see Dozier 1981; Daniels 2007). The primary advantage is that measurements taken are independently of emissivity and any assumptions about the kinetic temperature of the source. In fact, the apparent kinetic temperature is measured using this method, along with the emissivity–fractional fire area product, εA_f (Kremens *et al.* 2010). It should be noted that the FRFD measured using this method is representative of just the fractional hot areas within the field of view of the detector. Wooster *et al.* (2005) report FRFD estimates derived from near-source dual-band radiometry and details on the FRFD calculation method used in the present paper (involving a series of calibration and analysis steps) are given in Kremens *et al.* (2010).

A two-band radiometer relies on the fact that, for an assumed blackbody or greybody radiation source, the ratio between any two infrared bands is related to the kinetic temperature of the source. The blackbody/greybody assumption of the method will be violated if the fire is a selective emitter (e.g. if radiant energy is produced by molecular or atomic emission in narrow bands). It has long been known that CO_2 and other gaseous molecules (e.g. H_2O) emit energy in multiple bands of closely spaced, extremely spectrally narrow lines (Smyth 1931). Although the emission from each line is large, its contribution to emission integrated across a spectral region is small because the bands are spectrally narrow. Recently published fire emission spectra obtained from a Fourier-transform IR spectrometer (Boulet *et al.* 2009; Parent *et al.* 2010) would suggest the opposite, but only because the resolution of the instrument is coarse and does not resolve the actual line-emission structure. As well, we expect that the emission spectrum will more closely approach that of a greybody as the perspective of the detector approaches nadir because of the inclusion of hot fuel particles in the field of view of the detector (Parent *et al.* 2010) and the heated soil surface underneath the combustion zone (Kremens *et al.* 2003). A basic molecular physics calculation of the emissive power of these line emission sources remains to be done for wildland fuel combustion.

Ignition along the upwind side of the plots (outside of the field-of-view of the detector) was accomplished via light application of a flaming diesel–gasoline mixture from a drip-torch ignition device applied from one corner of the plot to another at a brisk walking speed. By altering the speed of ignition at points along the plot, the fire was caused to progress in an orderly straight line through the radiometer's field of view. Two plots were used, with identical instrumentation, and the experiments alternated between one plot and another to speed up the data collection process. Between experiments, the ground under each plot was allowed to cool to ambient temperature and the ash blown away with leaf blowers. The soil beneath the plots was a flat mixture of compacted clay soil and gravel. A total of 12 experiments were performed over a range of fuel loadings

expected in the oak hardwood forests characteristic of the eastern United States (see Bova and Dickinson 2008).

Instrumentation description and calibration procedure

The main instrument used for flux determination in this experiment was a two-band infrared radiometer. The electronics for the radiometer were constructed in-house and were tested thoroughly for stability, heat resistance and accuracy. The instrument consists of two single-element thermopile detectors, amplifiers, filters and power conditioners. These components are mounted on a small printed circuit board that is housed in a fireproof housing. One detector (TPS334, Perkin Elmer Optoelectronics, Santa Clara, CA) has a silicon long-pass window that transmits from 5.5 to 15 µm, whereas the other detector (2M Dexter Research Inc., Dexter, MI) has a CaF_2 window with transmission from 0.2 to 9 µm. One of the thermopiles (TPS334) has an integral thermistor to monitor and correct for the effects of finite sensor temperature.

The instrument was calibrated in our laboratory using several Omega Corporation blackbody reference sources that span temperature ranges from 373 to 1300 K. We checked the instruments after exposure to the fire experiments and found no appreciable change in calibration. We have built ∼50 of these sensor heads, which have been used successfully not only on the small-plot fire experiments described here but also on prescribed fires in Georgia, Florida, Kentucky and Ohio that ranged from 20 to 1000 ha. These detectors have been cross-checked against other total-power detectors (e.g. 12-550 Precision Radiometer, Infrared Systems Development Corporation, Winter Park, FL, and Schmidt-Boelter radiometer, Medtherm Corporation, Huntsville AL).

Integrated heat budget

Acknowledging uncertainty in the magnitude of the effective heat of combustion, the integrated heat budget can be rearranged:

$$Wh_C = WQ_P + \text{FLED} + \text{FRED} + \text{FCED} + E_S + Wh_C\varphi \quad (2)$$

Several constants are required in the integrated heat budget (Eqn 2). We used constants that are widely accepted in the literature. Ash fraction for black oak litter (0.035, Susott 1982) was used along with fuel moisture content to estimate ash- and moisture-free fuel consumption. We used Susott's (1982) high heat of combustion (21.3 MJ kg^{-1}) for black oak foliage as estimated from the heats of combustion of volatiles and char, measured by bomb calorimetry, and the fraction of fuel that formed char. We defined the fuel preheating and pyrolysis enthalpy as:

$$WQ_P = W(Q_{pyr} + Mc_w(100 - T_a)) \quad (3)$$

where Q_{pyr} was assumed constant at 0.7 MJ kg^{-1} (Wilson 1985), M is weighted-average fuel moisture fraction by dry weight for the fuel bed (with weighting by fuel class), c_w is the specific heat of water (0.0042 MJ kg^{-1} °C^{-1}), and T_a is ambient temperature (set to 25°C). Latent energy in the plume (FLED) includes vapour from both fuel moisture and the combustion process.

$$\text{FLED} = W(MQ_V + Q_C) \quad (4)$$

Burn number	Moisture		Areal fuel consumption (kg m^{-2})		
	Litter	Wood	Litter	Wood	Total
4	11.7		0.15		0.15
10	7.3		0.30		0.30
3	12.4		0.30		0.30
5	12.4		0.30		0.30
1	7.6		0.35		0.35
2	8.7	21.7	0.30	0.10	0.40
9	7.6		0.57		0.57
6	11.4	23.4	0.50	0.39	0.89
7	13.6	27.4	0.81	0.70	1.52
8	10.2	15.4	0.61	1.43	2.05
11	10.3	13.0	0.92	2.13	3.04
12	9.7	13.8	0.92	2.33	3.25

where Q_V is the heat of vaporisation of water (2.25 MJ kg^{-1}) and Q_C is the latent energy of the water vapour generated from combustion of a unit mass of fuel (1.4 MJ kg^{-1}, Clements *et al.* 2006). At the fuel moisture contents observed in our experiments (Table 1), the latent heat from combustion far exceeds the heat of vaporisation of moisture in the fuel. A small fraction of the FRED is below the sensitivity of the instrument (for our instrumental setup, the threshold of detection is 0.140 kW m^{-2}). This threshold is approximately equal to the radiant power emitted as 'background radiation' from soils and fuel at ambient temperatures ($\sim$300 K) and can thus be ignored. Radiation interception by the atmosphere can also be ignored in these experiments because of the proximity of the sensor to the fire. As the experiments were conducted in an open space, radiation interception by the forest canopy was also not an issue as it would be for a sensor in an aircraft or satellite.

The convective and soil-heating components of the integrated fire heat budget (Eqn 2) were not measured and their estimation is beyond the scope of this study. We can combine these unknowns and estimate their magnitude using the following relationship:

$$E_U = \text{FCED} + E_S + W h_C \varphi \qquad (5)$$

where E_U is the unconstrained energy density (MJ m^{-2}) for which Eqn 2 can be solved. Consistent with other papers (e.g. Wooster *et al.* 2005; Freeborn *et al.* 2008), the fractional contribution by any of the various energy sinks and forms of energy dissipation to total energy generated by the fire can be obtained by ratio with the total combustion energy (the left-hand side of Eqn 2).

Results

Fuel consumption (ash- and moisture-free) ranged from 0.15 to 3.25 kg m^{-2} ($\sim$0.7–14.5 tons per acre, Table 1), a range

intended to span the expected consumption across the mixed-oak forests where major canopy disturbances (e.g. ice storms) had not occurred and where aircraft-based infrared mapping of prescribed fires was planned. The rate of spread estimated from the overhead camera ranged from 0.009 to 0.133 m s^{-1}. The overhead video was used to estimate rate of spread and these estimates compared well with rate of spread estimated from the thermocouple array (Bova and Dickinson 2008). Although video imagery from three perspectives was collected during the experiments and was orthorectified to provide a three-dimensional perspective, it was easier to use imagery from a single overhead perspective to estimate flame rates of spread. Fractional contributions of the various components of the integrated heat budget to dissipation of total combustion energy are shown in Table 2 and Fig. 4. Note that E_U is not estimated independently, but is the difference between the left-hand sides of Eqn 5 and Eqn 2 after other terms are estimated. For reasons of parsimony, a linear model was used to describe the relationship between FRED and fuel consumption (Fig. 5).

Byram's (1959) fireline intensity is the product of fuel consumption, fuel bed combustion energy (h_C) and rate of spread, and it ranged from 151 to 813 kW m^{-1} in our experiments. Flame lengths calculated from fireline intensity by the relationship of Weise and Biging (1996) ranged from 0.5 to 1.8 m, which agreed well with video observations of the fires. As would be expected, peak FRFD is positively related to fireline intensity (Fig. 6). It would be tempting to calculate a flaming zone depth from the ratio of fireline intensity and peak FRFD. However, peak FRFD is an instantaneous measurement and fireline intensity is an integrated measurement from ignition through cooling. Thus, Fig. 6 is more properly an empirical relationship by which, through inversion, rough estimates of fireline intensity might be made. In contrast, there is no straightforward relationship between radiative fraction and either fireline intensity or fuel consumption (Fig. 7*a*, *b*).

Discussion

We have estimated the FRED and FRFD in experiments in small plots (18.5 m^2). However, challenges remain in understanding fire radiation. For example, it is unclear whether the assumption of hemispherical isotropy of radiation from a flaming front is valid (Kremens *et al.* 2010). In experiments by Freeborn *et al.* (2008), radiation measurements from the same instrument at increasing angles from vertical were not equal for an $\sim$1-m scale (subpixel) fire. Measurements and modelling would also test the isotropy assumption for the radiation that causes soil heating.

Fire radiative fraction was estimated to be 0.17 (s.d. = 0.03) in our experiments on the basis of total theoretical combustion energy (i.e. the left side of Eqn 2). For purposes of comparison, using the estimate of 0.368 kg MJ^{-1} (fuel consumption per unit of radiated energy) of Wooster *et al.* (2005) from outdoor, small-plot burns and the estimate of 0.453 kg MJ^{-1} for indoor fires of Freeborn *et al.* (2008), we calculated the corresponding radiative fractions from our consumption data. To estimate consumption, we included ash and 7% fuel moisture for Wooster *et al.* (2005) and ash and no fuel moisture for Freeborn *et al.* (2008). Then, using the above yields to estimate FRE, we arrived at radiative fractions of 0.14 and 0.11 respectively. Because of a

Table 2. Components of the integrated fire heat budget (Eqn 2)

Total combustion energy (Wh_C) is the left side of Eqn 2 using areal fuel consumption from Table 1. WQ_P is the areal fuel preheating and pyrolysis enthalpy but does not include the heat of vaporisation of fuel moisture (Eqn 3). FLED is the combined heat of condensation of fuel moisture and water vapour produced by combustion (Eqn 4). FRED is fire radiated energy density and E_U includes areal fire convective energy and soil heating (Eqn 5). All terms are in units of MJ m^{-2} with fraction of total combustion provided to the right of each term from the integrated heat budget. Burns are ordered by increasing consumption

| Burn number	Wh_C	WQ_P	Fraction WQ_P	FLED	Fraction FLED	FRED	Fraction FRED	E_U	Fraction E_U
4	3.2	0.11	0.035	0.25	0.078	0.42	0.13	2.43	0.76
10	6.4	0.22	0.035	0.47	0.074				
3	6.4	0.022	0.035	0.50	0.079	0.97	0.15	4.69	0.73
5	6.4	0.22	0.035	0.50	0.079	1.03	0.16	4.62	0.72
1	7.5	0.25	0.034	0.55	0.074				
2	8.4	0.29	0.035	0.66	0.078	1.82	0.22	5.65	0.67
9	12.2	0.42	0.034	0.90	0.074				
6	19.1	0.68	0.035	1.59	0.084				
7	32.3	1.16	0.036	2.81	0.087	6.78	0.21	21.53	0.67
8	43.5	1.52	0.035	3.50	0.081	6.88	0.16	31.61	0.73
11	64.7	2.25	0.035	5.10	0.079	9.99	0.15	47.39	0.073
12	69.1	2.40	0.035	5.47	0.079	9.80	0.014	51.4	0.074
Average			0.035		0.079		0.17		0.72
Standard deviation			0.0005	0	0.004		0.03		0.03
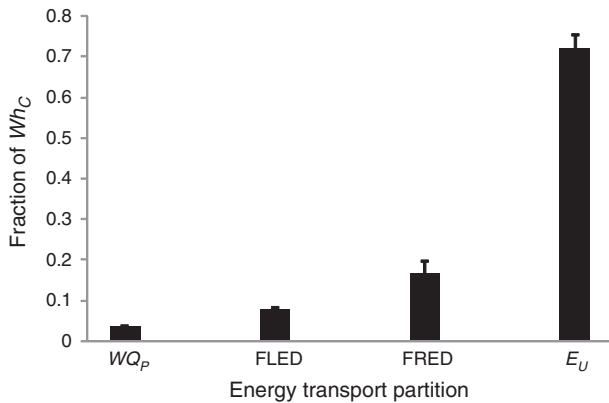
Fig. 4. Partition of energy transport (see Table 2). Fractional contributions (+1 s.d.) on the basis of total combustion energy (left side of Eqn 2) are shown.

Fig. 5. Areal fuel consumption *v.* fire radiative energy density (FRED) for this experiment and literature. See text for a description of the rescaling required for Wooster *et al.* (2005) and Freeborn *et al.* (2008) in order that fuel consumption from all three studies could be compared on a moisture- and ash-free basis.

standard deviation of ~0.03 in the radiative fraction estimates of Wooster *et al.* (2005) and Freeborn *et al.* (2008), we can conclude that the confidence interval for the estimate of Wooster *et al.* (2005) overlaps with ours, whereas that of Freeborn *et al.* (2008) may be lower (see below). Wooster *et al.* (2005) and Freeborn *et al.* (2008) found a monotonic increase in radiative fraction with fuel consumption in contrast with our more ambiguous, possibly parabolic, relationship over a similar range in fuel consumption (Fig. 7*a*, *b*). We can only speculate on the reason for the difference between their non-spreading fires and our spreading fires. It would be interesting to know whether and how the partitioning of combustion energy between radiation and convection varies in spreading fires as fireline intensity increases over a range larger than that in our experiments. Also, convective fraction is expected to decline with increases in combustion efficiency (W. Mell, pers. comm.).
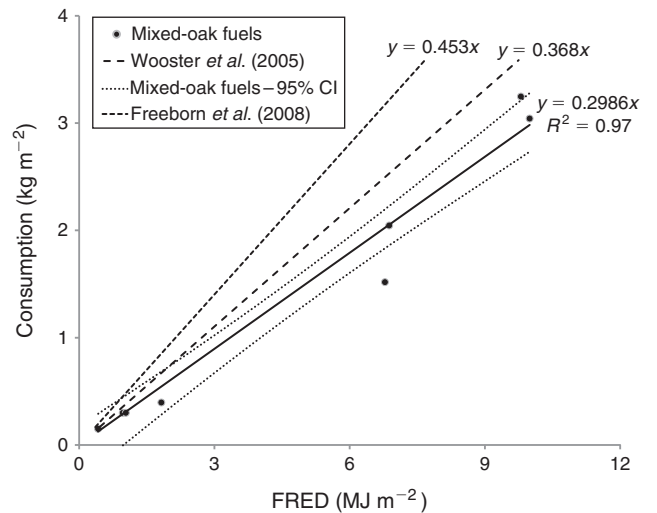
Uncertainty in the magnitude of the radiative fraction resides in uncertainty in heats of combustion. Estimates of total (high) heats of combustion were 21.3, 17.1–19.4 and 17.9–22.5 MJ kg^{-1} in our study, Wooster *et al.* (2005) and Freeborn *et al.* (2008). The heat of combustion we used was at the high end of the range (and was chosen to represent leaf litter, the fine fuel that carried the fires). Including wood heats of combustion would have had little to no effect on our estimates of radiative fraction because wood heats of combustion are similar to our foliage heats of combustion (e.g. Susott 1982). As or more important than estimates of high heats of combustion is the fact that high heats of combustion are effectively reduced by incomplete gas-phase
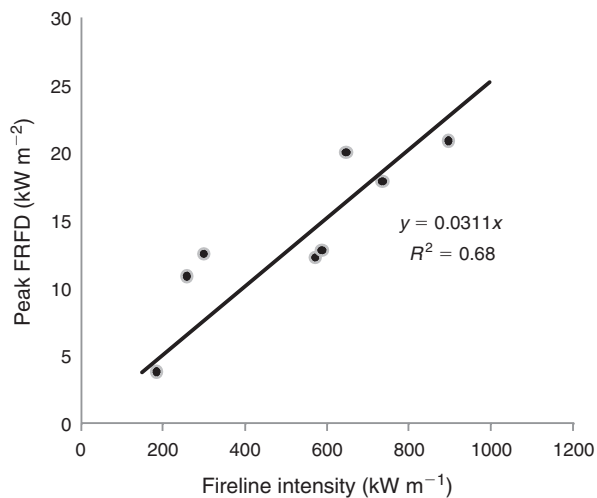
Fig. 6. Peak fire radiative flux density (FRFD) *v.* Byram's fireline intensity. See text for fireline intensity calculation method.

combustion and formation of unconsumed char. This uncertainty is reflected in the E_U term in our heat budget (Eqn 5). Babrauskas (2006) found that effective heats of combustion declined with foliage moisture content and were estimated to be 70% of high heats of combustion in tests with conifers that were recently cut (i.e. green) and cured to provide a range of foliage moisture contents. Propensity to char varies considerably among fuels (Susott 1982; Dietenberger 2002) and also will affect the effective heat of combustion.

The present measurement technique, using a dual-band infrared radiometer, has significant advantages over the methods employed on previous experiments. Wooster *et al.* (2005) found that FRP estimates from a single mid-wavelength infrared (MWIR) band were lower than those estimated from a dual-band estimation method. Freeborn *et al.* (2008) used a single-band imaging radiometer sensitive in the MWIR, which may explain their lower radiative fraction estimates. Knowing only the sensor-reaching radiance in a single narrow waveband, it is difficult to determine the total infrared flux accurately without also making assumptions about the temperature and emissivity of the source. Using two or more bands allows determination of the source temperature as well as the emissivity–area product for the restricted case of a detector field-of-view occupied partially by a high-temperature source (fire) and partially by a cold (low exitance) source (see Kremens *et al.* 2010). Riggan *et al.* (2000) consider sensitivities and potential pitfalls of the dual-band method for remote sensing of wildland fires.

Freeborn *et al.* (2008) calculated the convective heat release using mass flow rate and temperature differences within the exhaust stack to determine that the fraction of total combustion energy (based on high heat of combustion) released by convection was 0.56 for their $\sim$1-m^2 fires (value rescaled to fuel on a moisture- and ash-free basis). We estimate that the fraction of total energy accounted for by convection, soil heating and combustion inefficiency is 0.72 (s.d. = 0.03, Table 2). Assuming $\sim$10% moisture content of our consumed fuels and Babrauskas' (2006) relationship between effective heat of combustion and (live) fuel moisture content (his equation 3) we might expect to
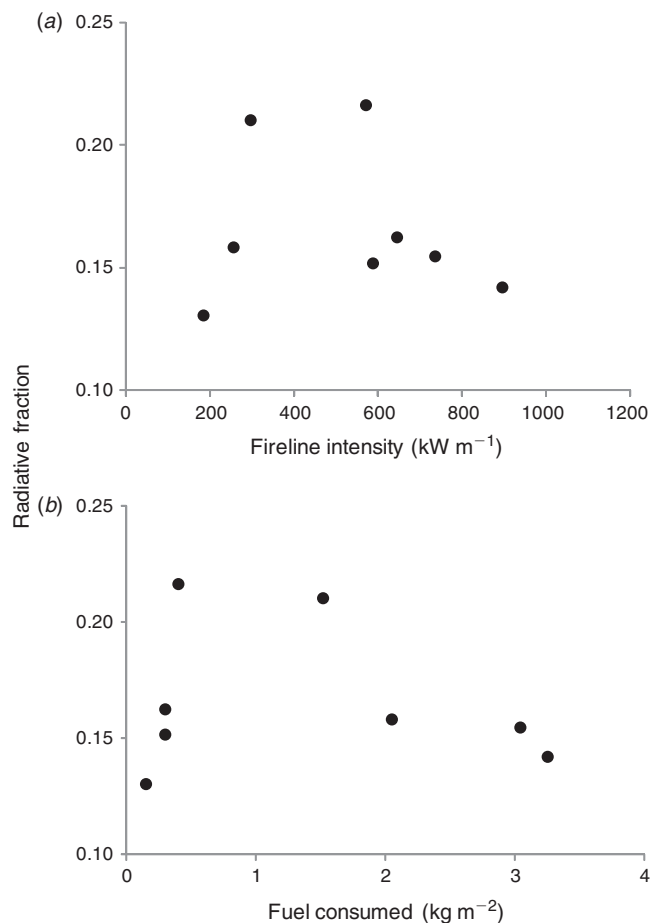

Fig. 7. (*a*) Radiative fraction *v.* Byram's fireline intensity. See text for fireline intensity calculation method. (*b*) Radiative fraction *v.* aerial fuel mass consumed.

see a combustion inefficiency of $\sim$2.3 MJ kg^{-1} or $\sim$11% (relative to high heat of combustion) and, thus, the fraction of total combustion energy accounted for by convection and soil heating would be $\sim$0.61. Using the estimate of Wooster *et al.* (2005) that heat dissipation to the soil was $\sim$25% of FRE, we can estimate that the fraction of convective energy dissipation in our experiments was $\sim$0.57 (s.d. 0.04), no different from the estimate of Freeborn *et al.* (2008) for small-scale, non-spreading fires in a laboratory setting.

Most measurements of the convective field have focussed on flux densities (kW m^{-2}) (Clark *et al.* 1999; Coen *et al.* 2004; Clements *et al.* 2006) and not estimates of integrated heat release (kJ m^{-2}) from ignition through extinction. In contrast to measurement of wildland fire radiation, where aerial measurement may be made over event scales using airborne sensors, current techniques for estimating fire convective flux and (through integration) energy in the field only provide point estimates of convective flux. Convective flux measurement are further complicated because of limitations imposed by the high heat fluxes and wildly varying gas temperatures within the fire environment. Simultaneous measurement of convective and radiative flux and energy in a field environment remains a

daunting challenge. Methods for estimating convective heat flux including high-frequency infrared video (e.g. Clark *et al.* 1999; Radke *et al.* 2000; Coen *et al.* 2004), sonic anemometry at some height in the plume at which gas temperatures do not exceed measurement device physical limitations (Clements 2007), and pressure-transducing devices that estimate flow in and near flames (McCaffrey and Hekestad 1976; B. Butler, pers. comm) are all promising. There would seem to be value in the expanded use of Doppler LiDAR and RADAR for characterising event-scale convective dynamics (Banta *et al.* 1992).

Soil heating and latent heat losses should also be quantified in future integrative experiments. Energy dissipated by soil heating was on the order of 25% of the radiated energy in the experiments of Wooster *et al.* (2005), but it is an important quantity ecologically (Massman *et al.* 2010) and should be measured under a wider range of conditions. Latent heat losses can be estimated from fuel consumption and fuel moisture, but can also be measured directly in the plume (Clements *et al.* 2006).

Constraining the fire heat budget, both instantaneous and integrated, will benefit fire propagation modelling efforts (e.g. Mell *et al.* 2007). Although FRFD and FRED can be measured continuously over large areas (e.g. Radke *et al.* 2000; Riggan *et al.* 2004), measurements of convective and other fluxes are limited in their utility for comparison with model output because they are typically point estimates and minimally replicated. As we have shown, and for reasons we do not understand, the radiative fraction may vary widely with combustion conditions (Fig. 7*a*, *b*). Consequently, improving modelling efforts will also require simultaneous measurements of radiative, convective and conductive fluxes along with fuel consumption and fire spread behaviour. For the near term, these convective and other flux measurements will have to be made at a much greater number of points in a fire than has been done to date, requiring development of inexpensive, small sensors that are easy to deploy. Only exploratory measurements of the radiation field at event scales and high temporal resolution have been conducted (e.g. Radke *et al.* 2000) and most measurements have had very limited time resolution (e.g. only a few samples during the duration of the fire; e.g. Riggan *et al.* 2004). Good models, based on sound physics and tested at laboratory and plot scales, may be the only way to understand the energy budget of an event-scale fire in the near term and model use should be integrated with measurement campaigns.

Summary and conclusions

By coordinated measurement of fuel consumption and fire radiative power and energy for spreading fires at an intermediate scale ($\sim$18.5 m^2), we strengthen the link between fire behaviour and the remotely sensed, event-scale radiative field. In exploring an integrated fire heat budget, we highlight the need for coordinated measurements and modelling of heat generation and the various forms of heat dissipation on spreading fires. The rank order in the fraction of total combustion energy accounted for by different sinks and dissipation modes in the integrated heat budget ranged from convective (sensible) heat release and soil heating combined, to radiation, to the latent energy of vapour produced by combustion and vapourised fuel moisture,

and to the enthalpy of fuel preheating and pyrolysis. The integrated heat budget unfolds in a control volume in which heat is exchanged among its radiative, convective and soil-heating components. Thus, a combination of high-temporal-resolution measurement, laboratory determinations of effective heats of combustion under different conditions and process modelling is needed to constrain heat dissipation in the dynamic fire front as it interacts with the atmosphere. Describing the radiation field currently provides the greatest potential for extrapolating plot-scale dynamics to events, allowing us to better understand fire–atmosphere coupling and ecological effects at a scale relevant for management.

References

Babrauskas V (2006) Effective heat of combustion for flaming combustion of conifers. *Canadian Journal of Forest Research* **36**, 659–663. doi:10.1139/X05-253

Banta RM, Olivier LD, Holloway ET, Kropfli RA, Bartram BW, Cupp RE, Post MJ (1992) Smoke-column observations from two forest fires using Doppler Lidar and Doppler radar. *Journal of Applied Meteorology* **31**, 1328–1349. doi:10.1175/1520-0450(1992)031<1328:SCOFTF>2.0.CO;2

Boulet P, Parent G, Collin A, Acem Z, Porterie B, Clerc JP, Consalvi JL, Kaiss A (2009) Spectral emission of flames from laboratory-scale vegetation fires. *International Journal of Wildland Fire* **18**, 875–884. doi:10.1071/WF08053

Bova AS, Dickinson MB (2008) Beyond 'fire temperatures': calibrating thermocouple probes and modeling their response to surface fires in hardwood fuels. *Canadian Journal of Forest Research* **38**, 1008–1020. doi:10.1139/X07-204

Byram GM (1959) Combustion of forest fuels. In 'Forest Fire: Control and Use'. (Ed. KP Davis) pp. 61–89. (McGraw-Hill: New York)

Clark TL, Radke L, Coen J, Middleton D (1999) Analysis of small-scale convective dynamics in a crown fire using infrared video camera imagery. *Journal of Applied Meteorology* **38**, 1401–1420. doi:10.1175/1520-0450(1999)038<1401:AOSSCD>2.0.CO;2

Clements CB (2007) FIREFLUX – observing wildland grass fire dynamics. *Bulletin of the American Meteorological Society* **88**, 1369–1382. doi:10.1175/BAMS-88-9-1369

Clements CB, Potter BE, Zhong S (2006) *In situ* measurements of water vapor, heat, and CO$_2$ fluxes within a prescribed grass fire. *International Journal of Wildland Fire* **15**, 299–306. doi:10.1071/WF05101

Clements CB, Zhong S, Bian X, Heilman WE, Byun DW (2008) First observations of turbulence generated by grass fires. *Journal of Geophysical Research* **113**, D22102. doi:10.1029/2008JD010014

Coen J, Mahalingam S, Daily J (2004) Infrared imagery of crown-fire dynamics during FROSTFIRE. *Journal of Applied Meteorology* **43**, 1241–1259. doi:10.1175/1520-0450(2004)043<1241:IIOCDD>2.0.CO;2

Daniels A (2007) 'Field Guide to Infrared Systems.' (SPIE Publishing: Bellingham, WA)

Dickinson MB, Ryan KC (2010) Strengthening the foundation of wildland fire effects prediction for research and management – introduction to the special issue. *Fire Ecology* **6**, 1–12. doi:10.4996/FIREECOLOGY.0601001

Dietenberger MA (2002) Update for combustion properties of wood components. *Fire and Materials* **26**, 255–267. doi:10.1002/FAM.807

Dozier J (1981) A method for satellite identification of surface temperature fields of sub-pixel resolution. *Remote Sensing of Environment* **11**, 221–229. doi:10.1016/0034-4257(81)90021-3

Freeborn PH, Wooster MJ, Hao WM, Ryan CA, Nordgren BL, Baker SP, Ichoku C (2008) Relationships between energy release, fuel mass loss and trace gas and aerosol emissions during laboratory biomass fires. *Journal of Geophysical Research* **113**. doi:10.1029/2007JD008679

Kaufman Y, Remer L, Ottmar R, Ward D, Rong RL, Kleidman R, Fraser R, Flynn L, McDougal D, Shelton G (1996) Relationship between remotely sensed fire intensity and rate of emission of smoke: SCAR-C experiment. In 'Global Biomass Burning.' (Ed. J Levine) pp. 685–696 (MIT Press: Cambridge, MA)

Kremens RL, Faulring J, Hardy C (2003) Measurement of the time–temperature and emissivity history of the burn scar for remote sensing applications. In 'Proceedings of the Second International Wildland Fire Ecology and Fire Management Congress and Fifth Symposium on Fire and Forest Meteorology', 16–20 November 2003, Orlando, FL. p. J1G.5 (American Meteorological Society: Boston, MA)

Kremens RL, Smith AMS, Dickinson MB (2010) Fire metrology: current and future directions in physics-based measurements. *Fire Ecology* **6**, 13–35.

Massman WJ, Frank JM, Mooney SJ (2010) Advancing investigation and physical modeling of fire effects on soils. *Fire Ecology* **6**, 36–54. doi:10.4996/FIREECOLOGY.0601036

McCaffrey BJ, Hekestad G (1976) A robust bidirectional low-velocity probe for flame and fire application. *Combustion and Flame* **26**, 125–127. doi:10.1016/0010-2180(76)90062-6

Mell W, Jenkins MA, Gould J, Cheney P (2007) A physics-based approach to modelling grassland fires. *International Journal of Wildland Fire* **16**, 1–22. doi:10.1071/WF06002

Parent G, Acem Z, Lechene S, Boulet P (2010) Measurement of infrared radiation emitted by the flame of a vegetation fire. *International Journal of Thermal Sciences* **49**, 555–562. doi:10.1016/J.IJTHERMALSCI.2009.08.006

Radke LR, Clark TL, Coen JL, Alther C, Lockwood RN, Riggin PJ, Brass JA, Higgins RG (2000) The Wildfire Experiment (WiFE): observations with airborne remote sensors. *Canadian Journal of Remote Sensing* **26**, 406–417.

Riggan PJ, Hoffman JW, Brass JA (2000) Estimating fire properties by remote sensing. In 'Aerospace Conference Proceedings, 2000 IEEE', 18–25 March 2000, Big Sky, MT, vol. 3, pp. 173–179. doi:10.1109/AERO.2000.879845

Riggan PJ, Tissell RG, Lockwood RN, Brass JA, Pereira JAR, Miranda HS, Miranda AC, Campos T, Higgins R (2004) Remote measurement of energy and carbon flux from wildfires in Brazil. *Ecological Applications* **14**, 855–872. doi:10.1890/02-5162

Roberts G, Wooster MJ, Perry GLW, Drake N, Rebelo LM, Dipotso F (2005) Retrieval of biomass combustion rates and totals from fire radiative power observations: application to southern Africa using geostationary SEVIRI imagery. *Journal of Geophysical Research* **110**, D21111. doi:10.1029/2005JD006018

Roberts GJ, Wooster MJ (2008) Fire detection and fire characterization over Africa using Meteosat SEVIRI. *IEEE Transactions on Geoscience and Remote Sensing* **46**, 1200–1218. doi:10.1109/TGRS.2008.915751

Smyth HD (1931) The emission spectrum of carbon dioxide. *Physical Review* **38**, 2000–2015. doi:10.1103/PHYSREV.38.2000

Susott RA (1982) Characterization of the thermal properties of forest fuels by combustible gas analysis. *Forest Science* **28**, 404–420.

Weise DR, Biging GS (1996) Effects of wind velocity and slope on flame properties. *Canadian Journal of Forest Research* **26**, 1849–1858. doi:10.1139/X26-210

Wilson RA (1985) Observations of extinction and marginal burning in free-burning porous fuel beds. *Combustion Science and Technology* **44**, 179–193. doi:10.1080/00102208508960302

Wooster MJ, Roberts G, Perry GLW, Kaufman YJ (2005) Retrieval of biomass combustion rates and totals from fire radiative power observations: 1. FRP derivation and calibration relationships between biomass consumption and fire radiative energy release. *Journal of Geophysical Research* **110**, D24311. doi:10.1029/2005JD006318